DNA Rotaxane Shuttles

DOI: 10.1002/anie.201405447

Logic Gating by Macrocycle Displacement Using a Double-Stranded DNA [3]Rotaxane Shuttle**

*Finn Lohmann, Johannes Weigandt, Julián Valero, and Michael Famulok**

Dedicated to Professor Javier de Mendoza on the occasion of his 70th birthday

Abstract: *Molecular interlocked systems with mechanically trapped components can serve as versatile building blocks for dynamic nanostructures. Here we report the synthesis of unprecedented double-stranded (ds) DNA [2]- and [3]rotaxanes with two distinct stations for the hybridization of the macrocycles on the axle. In the [3]rotaxane, the release and migration of the "shuttle ring" mobilizes a second macrocycle in a highly controlled fashion. Different oligodeoxynucleotides (ODNs) employed as inputs induce structural changes in the system that can be detected as diverse logically gated output signals. We also designed nonsymmetrical [2]rotaxanes which allow unambiguous localization of the position of the macrocycle by use of atomic force microscopy (AFM). Either light irradiation or the use of fuel ODNs can drive the threaded macrocycle to the desired station in these shuttle systems. The DNA nanostructures introduced here constitute promising prototypes for logically gated cargo delivery and release shuttles.*

Since the advent of DNA nanotechnology almost three decades ago,[1] increasingly complex two- and three-dimensional DNA nanostructures have been reported.[2] Due to the highly modular, flexible, and programmable nature of DNA, well-defined structural and functional assemblies can be created almost intuitively. While the fundamental principles for the structural assembly are basically understood, the current focus of the field now lies on constructing new biohybrid structures, the incorporation of diverse functionalities into these nanostructures, and their application for increasingly complex dynamic processes. Indeed, in the last decade, functional devices that operate by controlling DNA hybridization have progressed considerably, largely owing to the emergence of DNA origami technology.[3] Several dynamic DNA nanostructures like switches, stepped walkers, and tweezers have been reported, showing that mechanical motion can be controlled to achieve different functions such as the transport of cargo, the movement along pre-defined paths, and catalysis.[2] The stimuli employed for triggering these devices range from switching by toehold mechanisms to changes in pH, ions, and light wavelength.

Interlocked DNA nanostructures like catenanes[4] and rotaxanes[5] have been widely used for constructing molecular machines and devices due to their intrinsic ability to switch between different states without falling apart into individual components.[6] DNA [2]- and [3]catenanes and [2]rotaxanes proved to be ideal systems for incorporating dynamic properties into DNA nanostructures. Recently, we described a DNA rotaxane in which the mobility of the macrocycle can be switched on and off by alternating irradiation with UV and visible light, respectively.[7] Willner et al. recently reported a hybrid DNA/nanoparticle rotaxane structure that is able to translocate the interlocked macrocycle between two positions upon the addition of fuel oligodeoxynucleotides (ODNs).[5d]

Here we report the assembly and characterization of several dsDNA [2]- and [3]rotaxane-based shuttle systems.[8] Therein, one of the threaded macrocycles, the "shuttle ring", contains two single-stranded (ss) gap regions that recognize two hybridization sites, or "stations", also single-stranded, on the axle (Figure 1 a). By using either toehold release ODNs[9] or light irradiation we can control macrocycle hybridization selectively and translocate the shuttle ring from one station to the other. These shuttle control mechanisms were incorporated into various interlocked DNA nanostructures. By gel electrophoresis, AFM imaging, and fluorescence quenching (FQ) we then assessed the movement of the threaded macrocycles. We also demonstrate in a pilot study, how these dynamic systems might be employed for logic operations and DNA computing.

The design and assembly of the dsDNA [3]rotaxane structure is shown in Figure 1 a (for secondary structures and DNA sequences see Figure S1 and Table S1 in the Supporting Information). In this system, the shuttle ring is used to release the second ring in a strand-displacement cascade reaction, so that it finally dethreads from the interlocked structure. We chose this controlled disassembly to aid the unambiguous characterization of each different state of the cascade reaction that this highly modular and switchable nanostructure can go through.

Starting from the axle with two ss-gap regions, called station 1 (Figure 1 a, blue) and station 2 (green), two different dsDNA macrocycles[10] were threaded, a 105 base pair (bp)

[*] F. Lohmann, J. Weigandt, Dr. J. Valero, Prof. M. Famulok
Life and Medical Science (LIMES) Institute
Chemical Biology & Medicinal Chemistry Unit, University of Bonn
Gerhard-Domagk Strasse 1, 53121 Bonn (Germany)
E-mail: m.famulok@uni-bonn.de
Homepage: http://www.famuloklab.de
Prof. M. Famulok
Center of Advanced European Studies and Research (CAESAR)
Ludwig-Erhard-Allee 2, 53175 Bonn (Germany)

[**] This work was supported by grants from the European Research Council (ERC grant 267173), and the Alexander von Humboldt Foundation. We thank V. Adam for the synthesis of the DMAB-phosphoramidite.

Supporting information for this article is available on the WWW under http://dx.doi.org/10.1002/anie.201405447.

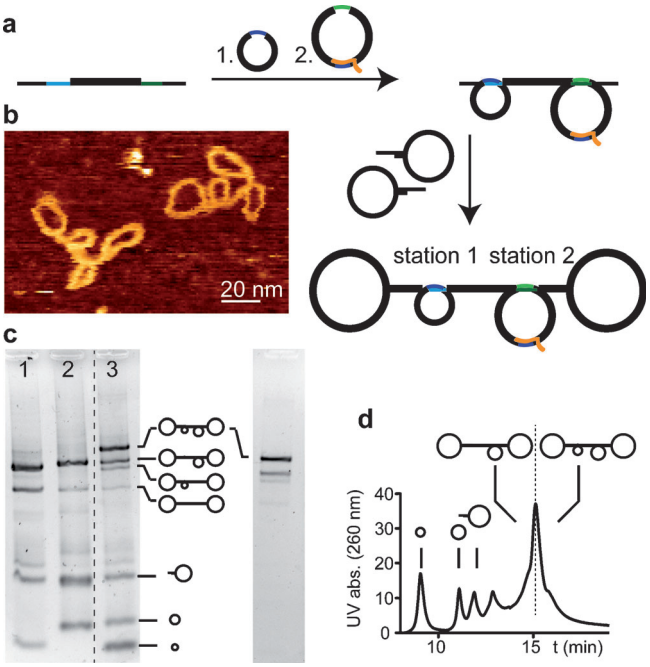

Figure 1. A Double-stranded DNA [3]rotaxane. a) Representation of the assembly of the [3]rotaxane. Stations on the axle are labeled cyan and green, the complementary ss-gaps on the two macrocycles are labeled blue and light green, respectively. b) AFM image of the [3]rotaxane recorded with high-resolution Hyperdrive mode in liquid. c) Analytical agarose gel of the rotaxanes with a single 105 bp ring (lane 1), single 126 bp ring (lane 2), both rings (lane 3), and the HPLC-purified [3]rotaxane (single lane). Entire gel left is shown in Figure S3 in the Supporting Information. d) HPLC chromatogram of the crude product. The majority of the right fraction of the main peak corresponds to the [3]rotaxane (see Figure 1 c, single lane).

ring with a ss-gap region complementary to station 1, and a 126 bp ring with a gap complementary to station 2. The 126 bp ring contains a second gap, complementary to station 1. To direct the hybridization of this ring to the desired position, this gap was blocked by hybridization to a blocking ODN (BO, orange). After both rings were threaded onto the axle, the stopper rings[5b] were added and ligated. Figure 1 c (left) shows the analytical agarose gel of the crude [3]rotaxane (lane 3). The [2]rotaxanes with either a single 105 bp ring (lane 1) or 126 bp ring (lane 2) were also assembled and used as references. Evidently, the [3]rotaxane is the predominant species although the corresponding [2]rotaxane side products are also formed. The crude product was purified by weak anion exchange HPLC (Figure 1 d). The [2]rotaxane with the 126 bp ring and the [3]rotaxane have similar retention times, hampering HPLC purification of the [3]rotaxane to homogeneity. Therefore, some residual amount of [2]rotaxane was observed in the analytical gel after purification (Figure 1 c, single lane). Nevertheless, this level of purity was sufficient for the full characterization of the structure by AFM and for performing the subsequent switching experiments. Indeed, AFM imaging with Hyperdrive in liquid (Figure 1 b and Figure S2) unequivocally confirms the predicted structure of the [3]rotaxane. To our knowledge, this is the first example of a DNA [3]rotaxane with two macrocycles threaded onto the axle. To study the versatility of this assembly, we also synthesized [3]rotaxanes with either one 168 and one 126 bp ring or with a 105 bp ring with two gaps and a 126 bp ring with one gap (analytical agarose gels: Figure S3). The diversity of nanostructures achieved by this modular approach opens the way to the creation of complex multicomponent systems with independent stimuli-response features.

We designed the [3]rotaxane so that the 126 bp ring can shuttle from one station to the other without dethreading, as 168 bp ring stoppers are known to maintain these rings interlocked for a certain period of time.[5a] Therefore, the BO (orange) hybridized to the station 1 gap in the shuttle ring was removed before the ring from station 2 was released. This line of action resulted in free movement of the shuttle ring along the axle. Rather than dethreading, the unblocked ss-gap of the shuttle ring hybridizes to station 1. Moreover, the ss-gap sequence was chosen such that the 105 bp ring is displaced when the 126 bp ring binds to station 1. Because the 105 bp ring can form only seven bases with station 1, whereas the shuttle ring docks to this site via 10 base pairs, binding of the latter is preferred. Apparently, the difference in free energy is sufficient for quantitative displacement of the smaller ring by the shuttle-ring. Without any hybridization site available, the 105 bp ring rapidly dethreads from the axle at 25 °C.

The switching process is illustrated in Figure 2 a. Starting from the purified [3]rotaxane (state 1) we triggered the system with two different input ODNs: input A removes the BO from its complementary gap in the shuttle ring that now can hybridize to station 1. Input B releases the shuttle ring from station 2. Thus, upon addition of only input A, the shuttle ring remains bound to station 2 leaving the [3]rotaxane nearly unaltered (state 2). In contrast, addition of only input B releases the shuttle ring still blocked by BO, preventing it from displacing the 105 bp ring. Instead, the shuttle ring dethreads, yielding a [2]rotaxane with the 105 bp ring bound to station 1 (state 4). When inputs A and B are added stepwise, the 126 bp ring is released to freely move along the axle, hybridize to station 1, and displace the 105 bp ring, which then dethreads. This results in a [2]rotaxane with the 126 bp ring on station 1 (state 3).

The lanes of the analytical agarose gel (Figure 2 b) represent the four possible states (1–4) depending on inputs A and B. Lane 1 corresponds to the [3]rotaxane without input ODNs, while lane 2 shows the [3]rotaxane in presence of input A. Both lanes show predominantly the [3]rotaxane and residual [2]rotaxane. In lane 2, a small shift of the bands is observed due to the loss of the blocking ODN (BO). In the presence of inputs A and B (lane 3), the main band corresponds to the [2]rotaxane with the shuttle ring threaded (state 3). When only input B is added (lane 4) a [2]rotaxane with the 105 bp ring (state 4) is formed. These results clearly indicate that the assembled system is triggered in the predicted way in a nearly quantitative fashion. To demonstrate that these bands correspond to the assigned [2]- and [3]rotaxanes, respectively, states 2–4 were analysed by AFM. Mainly [3]rotaxanes are observed in state 2, whereas in states 3 and 4 the [2]rotaxanes with one ring are the predominant species(Figure 2 c).

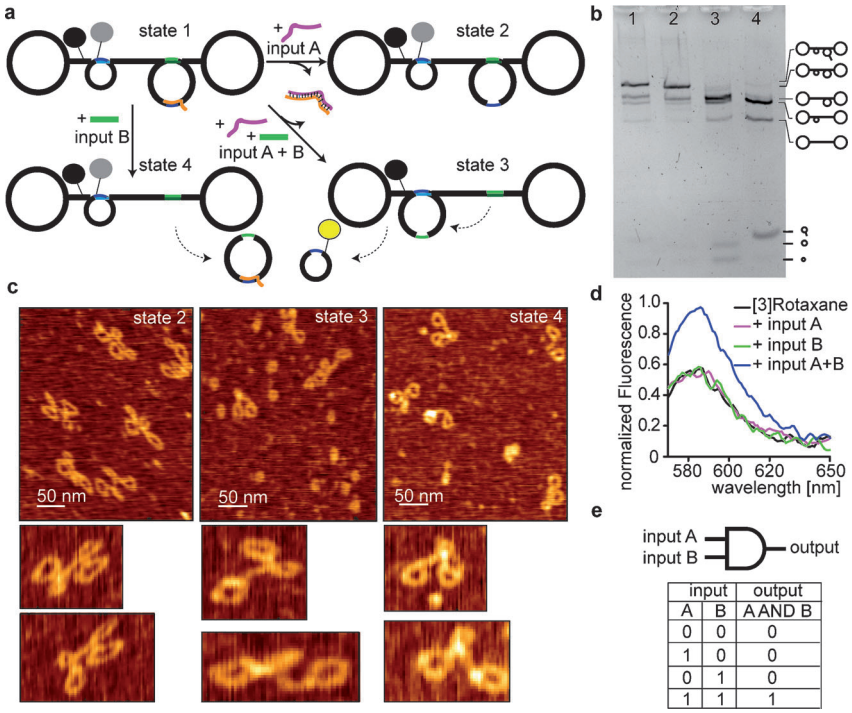

Figure 2. Operating the [3]rotaxane dethreading cascade. a) Representation of the [3]rotaxane response (state 1) to inputs A (pink) and B (green). Addition of input A removes the BO (orange) from the gap of the shuttle ring complementary to the blue station (state 2). Input B releases the 126 bp ring (state 4). Addition of inputs A and B unblocks and then releases the 126 bp ring which subsequently displaces the 105 bp ring (state 3). Fluorophore and quencher labels are indicated by filled circles (gray/yellow corresponds to TAMRA in quenched/unquenched state, black corresponds to the BHQ-2 label). b) Analytical agarose gel of the [3]rotaxane before (lane 1) and after addition of input A (lane 2), B (lane 3), and both A and B (lane 4). The dumbbells in the image of state 4 result from the residual [2]rotaxane present in the sample. c) AFM images of the [3]rotaxane in states 2–4. Entire AFM images are shown in Figure S4 in the Supporting Information. d) Fluorescence spectra of the sample before and after addition of input A, B, and both A and B. Fluorescence increases only after addition of input A and B, when the 105 bp ring is replaced by the 126 bp ring. e) Logic AND gate and corresponding truth table resulting from the fluorescence experiment with a threshold of 0.6 for the logic output (1/0).

input		output
A	B	A AND B
0	0	0
1	0	0
0	1	0
1	1	1

To prove that the 105 bp ring is released from the rotaxane only in presence of inputs A and B, and to observe the switching process in real time, we performed fluorescence-quenching (FQ) experiments. The 105 bp ring was labeled with the fluorophore TAMRA and the axle with the quencher BHQ-2. Threading of the ring quenches the TAMRA fluorescence due to its proximity to BHQ-2, whereas its release will separate the FQ pair and increase fluorescence. Figure 2d shows the fluorescence spectra of all four states. As expected, only inputs A and B together lead to a fluorescence increase. This system represents a logic AND gate with the corresponding increase in fluorescence as output (Figure 2d,e).

En route towards light-switchable inputs that respond to different wavelengths, we designed a dimethylazobenzene (DMAB) modified input B to activate/deactivate this input upon light irradiation (Figure 3b). Azobenzene (AB)-modified DNA forms stable duplexes with complementary strands when the AB residues are in the planar *trans* form, due to stabilizing stacking effects with the nucleobases.[11] Irradiation with UV light leads to isomerization into the nonplanar *cis* form, which destabilizes hybridization. Visible light reverts this process. Even higher switching efficiency is achieved when DMAB is used instead of AB.[7,12] Indeed, when we repeated the experiment shown in Figure 2 with a light-switchable DMAB-modified input B analogue, the same cascade reaction was triggered, as evidenced by gel electrophoresis (Figure S5).

To move towards a sophisticated reversible light-triggered shuttle, we designed a [2]rotaxane structure with two distinct stoppers at each end: a bulky spherical stopper, and a ring stopper. The nonsymmetric shape of the rotaxane facilitates the direct and unambiguous visualization of the translocation of the macrocycle from one station to the other by AFM imaging without requiring modification with markers like fluorophores or nanoparticles. To operate the light-triggered translocation of the shuttle ring between the two different ss stations on the axle, the eight-nucleotide-long station in close proximity to the ring stopper (Figure 3a, station 1, yellow) was modified with three DMABs at every second base position. Station 2 (Figure 3a, green) proximal to the spherical stopper was blocked with a DMAB-modified twelve-nucleotide-long release oligodeoxynucleotide (DMAB-5RO) containing five DMABs in total, one at every second base (Figure 3a; Figure S6 and Table S2 in the Supporting Information).

In step 1 of the [2]rotaxane assembly, DMAB-5RO was added to the axle to block station 2, followed by addition of the macrocycle containing gaps complementary to stations 1 and 2. After the ring had been threaded onto station 1 the spherical and ring stoppers were ligated to their respective sticky ends on the axle. Prior to the assembly, the DMAB-containing building blocks were isomerized into the *trans* form by irradiation at 450 nm. The final product was purified by weak anion exchange HPLC (Figure S7) and analyzed by agarose gel electrophoresis (Figure 3c).

High-resolution AFM analysis (Hyperdrive mode in liquid) revealed that the rotaxane formed as anticipated with the shuttle ring hybridized to station 1 (Figure 3d, top). Similarly, the [2]rotaxane was assembled without DMAB-5RO while station 1 was blocked simultaneously by irradiation at 365 nm. Again, AFM measurements corroborated that the shuttle ring was located at the predestined station 2 (Figure 3d, bottom). Not only does this analysis confirm the correct assembly but it also determines very precisely the exact position of the macrocycle on the axle before and after light switching.

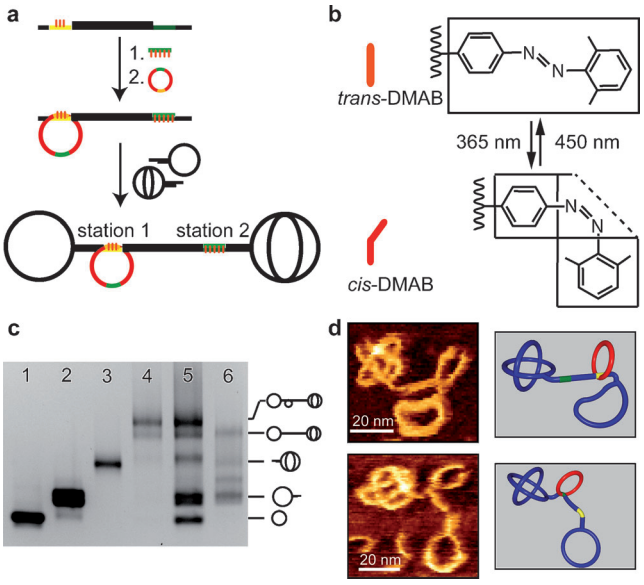

Figure 3. Light-switchable DNA [2]rotaxane with two addressable stations. a) Assembly of the nonsymmetric rotaxane. 1: DMAB-5RO; 2: 2-gap containing macrocycle. b) Chemical structures of *trans*- and *cis*-DMAB. c) Analytical agarose gel of the precursors (lane 1: macrocycle, lane 2: ring stopper, lane 3: spherical stopper) and the final HPLC-purified product (lane 4), the crude product (lane 5), and the nonsymmetric dumbbell that lacks the macrocycle (lane 6). d) AFM image of the nonsymmetric rotaxane shuttle recorded in Hyperdrive mode in liquid (left), and corresponding 3D representations of their arrangement on the modified cationic mica surface (right). Top panels: shuttle with the macrocycle on station 1; bottom panels: macrocycle on station 2.

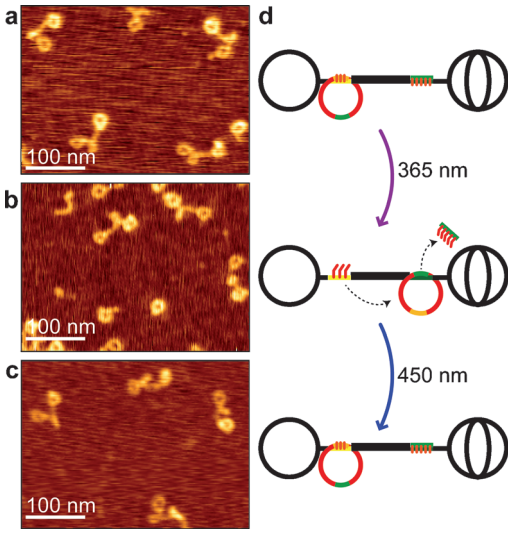

Figure 4. a–c) Representative AFM images of the light-switchable shuttle system before and after translocation of the macrocycle; images were recorded in AC mode in air. a) Before shuttling, ring on station 1. b) After irradiation with UV light, the ring moved to station 2. c) After subsequent irradiation with visible light, the ring relocates to station 1. d) Principle of the shuttling system. Orange bars indicate the *trans*-DMAB, kinked red bars the *cis*-DMAB.

Having characterized the two possible states of this system, we next analyzed the light switching mechanism itself. The principle of light-dependent shuttling between the two stations is illustrated in Figure 4d. After irradiation with visible light, the DMAB moieties isomerize into the *trans* form, resulting in blockage of station 2 by the DMAB-5RO. Simultaneously, the DMAB-modified station 1 enables macrocycle hybridization at this site (Figure 4d, top). When the system is exposed to UV light, *trans* to *cis* isomerization of DMAB occurs, thus releasing DMAB-5RO from station 2 and the macrocycle from station 1. Subsequently, the free macrocycle moves along the axle until it hybridizes to station 2, thus preventing it from dethreading. (Figure 4d, middle). Irradiation with visible light brings the macrocycle back to the starting position (Figure 4d, bottom).

To determine the potential reversibility of the system, we examined by AFM the repetitive shuttling of the macrocycle. Due to their three-dimensional shape, the spherical stoppers have a higher profile when absorbed to the mica surface and thus, exhibit a brighter color in the AFM images (Figure S8). We use this feature to assess the position of the macrocycle on the rotaxane axle. First, AFM images of the assembled rotaxane were recorded in AC mode. Almost all structures showed the shuttle ring correctly positioned on station 1 (Figure 4a, Figure S9). After irradiation at 365 nm, at least 75% of the intact rotaxane nanostructures showed the macrocycle correctly positioned on station 2 (Figure 4b, Figure S10). Finally, macrocycle relocation to station 1 occurred almost quantitatively after the system had switched back into the *trans* form (Figure 4c, Figure S11).

To conclude, our study reports the synthesis and characterization of several DNA [2]- and [3]rotaxane nanostructures. In these prototypes, interlocked macrocycles can shuttle between two positions embedded in the confined interlocked space. The assemblies and their various switching modes were characterized by analytical gel electrophoresis, AFM, and FQ. We employ the precise control of release and switching of the two macrocycles in the [3]rotaxane as a platform for DNA computing and show that the [3]rotaxane is able to perform logic AND operations using toehold and light-switchable ODNs as distinguishable inputs A and B. To achieve this, the system was designed such that macrocycle dethreading takes place in a cascade reaction that strictly depends on the sequence of input A and input B addition. To allow future expansion of the operational scope of this prototypic DNA nanostructure, we designed a DMAB-modified variant of input B that can be activated and deactivated by light irradiation. We show that reversible shuttling of a macrocycle between two stations can be achieved by irradiation with light at 365 nm and 450 nm. Light-triggered switching mechanisms have several advantages over other switching processes. For instance, the switching is carried out noninvasively only by irradiation with light. No fuel molecules need to be added that may pollute the system by accumulation of waste molecules or otherwise altering the system. Organic rotaxane arrays have previously been used for logic gating,[13] but these systems are likely less compatible for biocomputing than DNA-based devices.

The dynamic DNA nanostructures described here set the stage for more complex DNA computing devices that can be

operated by light control in a reversible fashion. Moreover, we envisage potential applications for the controlled release of DNA rings that carry bioactive molecules like DNAzymes, RNA kissing loops, chemical modifications, and drugs. It was shown previously that the dethreading time of the rings strongly depends on the ring and stopper sizes.[5a] Thus, the choice of appropriate pairs of stopper and macrocycle sizes may facilitate the fine-tuning and regulation of the release kinetics of multiple cargoes. The DNA-based shuttle systems described here may also allow to transport cargoes from a defined starting point to a distant end point on a longer DNA track containing more than two stations. The highly versatile nature of these interlocked DNA nanostructures, the variety of macrocycles, threading mechanisms, stopper molecules, and switching modes[7,14] provides a rich toolbox for applications in nanoengineering, DNA computing, and even nanomedicine.

Received: May 20, 2014
Published online: July 30, 2014

Keywords: DNA computing · DNA rotaxanes · nanostructures · molecular devices

[1] N. C. Seeman, *Annu. Rev. Biochem.* **2010**, *79*, 65 – 87.
[2] a) J. Bath, A. J. Turberfield, *Nat. Nanotechnol.* **2007**, *2*, 275 – 284; b) D. Y. Zhang, G. Seelig, *Nat. Chem.* **2011**, *3*, 103 – 113; c) L. Jaeger, A. Chworos, *Curr. Opin. Struct. Biol.* **2006**, *16*, 531 – 543; d) Y. Krishnan, F. C. Simmel, *Angew. Chem.* **2011**, *123*, 3180 – 3215; *Angew. Chem. Int. Ed.* **2011**, *50*, 3124 – 3156; e) F. C. Simmel, *Angew. Chem.* **2008**, *120*, 5968 – 5971; *Angew. Chem. Int. Ed.* **2008**, *47*, 5884 – 5887; f) F. C. Simmel, *Curr. Opin. Biotechnol.* **2012**, *23*, 516 – 521; g) S. S. Simmel, P. C. Nickels, T. Liedl, *Acc. Chem. Res.* **2014**, *47*, 1691; h) P. K. Lo, K. L. Metera, H. F. Sleiman, *Curr. Opin. Chem. Biol.* **2010**, *14*, 597 – 607; i) K. V. Gothelf, T. H. LaBean, *Org. Biomol. Chem.* **2005**, *3*, 4023 – 4037; j) K. V. Gothelf, R. S. Brown, *Chem. Eur. J.* **2005**, *11*, 1062 – 1069; k) C. M. Niemeyer, *Curr. Opin. Chem. Biol.* **2000**, *4*, 609 – 618; l) O. I. Wilner, I. Willner, *Chem. Rev.* **2012**, *112*, 2528 – 2556; m) T. J. Bandy, A. Brewer, J. R. Burns, G. Marth, T. Nguyen, E. Stulz, *Chem. Soc. Rev.* **2011**, *40*, 138 – 148; n) E. Stulz, G. Clever, M. Shionoya, C. Mao, *Chem. Soc. Rev.* **2011**, *40*, 5633 – 5635.
[3] a) P. W. K. Rothemund, *Nature* **2006**, *440*, 297 – 302; b) B. Saccà, C. M. Niemeyer, *Angew. Chem.* **2012**, *124*, 60 – 69; *Angew. Chem. Int. Ed.* **2012**, *51*, 58 – 66; c) A. Rajendran, M. Endo, H. Sugiyama, *Angew. Chem.* **2012**, *124*, 898 – 915; *Angew. Chem. Int. Ed.* **2012**, *51*, 874 – 890; d) A. Somoza, *Angew. Chem.* **2009**, *121*, 9570 – 9572; *Angew. Chem. Int. Ed.* **2009**, *48*, 9406 – 9408; e) T. Tørring, N. V. Voigt, J. Nangreave, H. Yan, K. V. Gothelf, *Chem. Soc. Rev.* **2011**, *40*, 5636 – 5646; f) A. Kuzuya, M. Komiyama, *Nanoscale* **2010**, *2*, 310 – 322; g) J. Nangreave, D. Han, Y. Liu, H. Yan, *Curr. Opin. Chem. Biol.* **2010**, *14*, 608 – 615; h) W. M. Shih, C. Lin, *Curr. Opin. Struct. Biol.* **2010**, *20*, 276 – 282.
[4] a) Y. Sannohe, H. Sugiyama, *Bioorg. Med. Chem.* **2012**, *20*, 2030 – 2034; b) J. Elbaz, Z. G. Wang, F. Wang, I. Willner, *Angew. Chem.* **2012**, *124*, 2399 – 2403; *Angew. Chem. Int. Ed.* **2012**, *51*, 2349 – 2353; c) C. H. Lu, A. Cecconello, J. Elbaz, A. Credi, I. Willner, *Nano Lett.* **2013**, *13*, 2303 – 2308; d) T. L. Schmidt, A. Heckel, *Nano Lett.* **2011**, *11*, 1739 – 1742; e) Y. Liu, A. Kuzuya, R. Sha, J. Guillaume, R. Wang, J. W. Canary, N. C. Seeman, *J. Am. Chem. Soc.* **2008**, *130*, 10882 – 10883; f) F. Lohmann, J. Valero, M. Famulok, *Chem. Commun.* **2014**, *50*, 6091 – 6093; g) T. Li, M. Famulok, *J. Am. Chem. Soc.* **2013**, *135*, 1593 – 1599; h) N. C. Seeman, J. H. Chen, J. E. Mueller, S. M. Du, Y. L. Wang, Y. W. Zhang, *FASEB J.* **1992**, *6*, A364 – A364; i) D. Han, S. Pal, Y. Liu, H. Yan, *Nat. Nanotechnol.* **2010**, *5*, 712 – 717.
[5] a) D. Ackermann, T. L. Schmidt, J. S. Hannam, C. S. Purohit, A. Heckel, M. Famulok, *Nat. Nanotechnol.* **2010**, *5*, 436 – 442; b) D. Ackermann, S. S. Jester, M. Famulok, *Angew. Chem.* **2012**, *124*, 6875 – 6879; *Angew. Chem. Int. Ed.* **2012**, *51*, 6771 – 6775; c) S. Bi, Y. Cui, L. Li, *Analyst* **2013**, *138*, 197 – 203; d) A. Cecconello, C. H. Lu, J. Elbaz, I. Willner, *Nano Lett.* **2013**, *13*, 6275 – 6280.
[6] S. S. Jester, M. Famulok, *Acc. Chem. Res.* **2014**, DOI: 10.1021/ar400321h.
[7] F. Lohmann, D. Ackermann, M. Famulok, *J. Am. Chem. Soc.* **2012**, *134*, 11884 – 11887.
[8] According to IUPAC nomenclature, these structures should be named pseudorotaxanes although hereafter, we will refer to them as rotaxanes for conciseness.
[9] B. Yurke, A. J. Turberfield, A. P. Mills, F. C. Simmel, J. L. Neumann, *Nature* **2000**, *406*, 605 – 608.
[10] a) G. Rasched, D. Ackermann, T. L. Schmidt, P. Broekmann, A. Heckel, M. Famulok, *Angew. Chem.* **2008**, *120*, 981 – 984; *Angew. Chem. Int. Ed.* **2008**, *47*, 967 – 970; b) D. Ackermann, G. Rasched, S. Verma, T. L. Schmidt, A. Heckel, M. Famulok, *Chem. Commun.* **2010**, *46*, 4154 – 4156.
[11] a) H. Asanuma, T. Ito, T. Yoshida, X. Liang, M. Komiyama, *Angew. Chem.* **1999**, *111*, 2547 – 2549; *Angew. Chem. Int. Ed.* **1999**, *38*, 2393 – 2395; b) H. Asanuma, X. Liang, H. Nishioka, D. Matsunaga, M. Liu, M. Komiyama, *Nat. Protoc.* **2007**, *2*, 203 – 212.
[12] H. Nishioka, X. Liang, H. Asanuma, *Chem. Eur. J.* **2010**, *16*, 2054 – 2062.
[13] a) C. P. Collier, E. W. Wong, M. Belohradsky, F. M. Raymo, J. F. Stoddart, P. J. Kuekes, R. S. Williams, J. R. Heath, *Science* **1999**, *285*, 391 – 394; b) A. R. Pease, J. O. Jeppesen, J. F. Stoddart, Y. Luo, C. P. Collier, J. R. Heath, *Acc. Chem. Res.* **2001**, *34*, 433 – 444.
[14] a) D. Ackermann, M. Famulok, *Nucleic Acids Res.* **2013**, *41*, 4729 – 4739; b) S. J. Green, D. Lubrich, A. J. Turberfield, *Biophys. J.* **2006**, *91*, 2966 – 2975; c) M. Wieland, A. Benz, J. Haar, K. Halder, J. S. Hartig, *Chem. Commun.* **2010**, *46*, 1866 – 1868; d) A. J. Turberfield, J. C. Mitchell, B. Yurke, A. P. Mills, Jr., M. I. Blakey, F. C. Simmel, *Phys. Rev. Lett.* **2003**, *90*, 118102; e) T. Liedl, H. Dietz, B. Yurke, F. Simmel, *Small* **2007**, *3*, 1688 – 1693.

